

Magnetic behaviour of Neodymium-substituted strontium hexaferrite

Bilal Hamid Bhat¹ · Basharat Want¹

Received: 28 November 2015 / Accepted: 30 January 2016 / Published online: 16 February 2016
© Springer-Verlag Berlin Heidelberg 2016

Abstract Neodymium-substituted strontium hexaferrites, $\text{Sr}_{1-x}\text{Nd}_x\text{Fe}_{12}\text{O}_{19}$ ($x = 0, 0.05, 0.10, 0.15, 0.20$), have been successfully synthesized by using citrate precursor method. The synthesized samples were characterized by X-ray diffraction, Transmission electron microscopy and vibrating sample magnetometry. The X-ray diffraction results show that the prepared samples are crystalline in nature and are of single phase with the space group $\text{P6}_3/\text{mmc}$. Transmission electron microscopy results show that the prepared sample is composed of fine nanoparticles with an average size of 80 nm. The effect on magnetic behaviour of strontium hexaferrite with neodymium substitution was analysed by using first-order reversal curves (FORCs). FORC analysis was done in order to know the domain state of magnetization of the nanoparticles and the nature of magnetic interactions among the particles. FORC diagrams depict a single peak, suggesting that the substituted systems are formed of interacting nanoparticles.

1 Introduction

M-type hexagonal ferrites represent a class of materials with promising technological importance in various fields such as magnetic recording, microwave devices, telecommunications and permanent magnets. These hexagonal ferrites possess large magnetocrystalline anisotropy, moderate energy product, high Curie temperature, excellent

chemical stability, higher corrosion and electrical resistivity [1, 2]. The properties of hexaferrite are sensitive to the preparation method, substitutions, sintering time and temperature, microstructure and largely on distribution of cations on the tetrahedral (*A*) and octahedral (*B*) sites [3]. A considerable enhancement of the magnetic properties of strontium hexaferrite can be obtained by small substitution of Sr^{2+} or Fe^{3+} ions or both [4] by several bi-, tri- and tetravalent ions. It has been reported that by substitution with rare-earth elements, various properties like thermal, electrical, magnetic and optical properties can be enhanced. There are several challenges related to the manufacturing of highly significant magnetic structures and the clear understanding of their magnetic behaviour. Recently, multiferroic quantum phase transitions have been studied in M-type hexaferrites, which have the simplest crystal structure among the rich family of hexagonal ferrites [5, 6].

Magnetization processes are usually examined by the analysis of the hysteresis curves and their various parameters such as saturation magnetization, coercivity and remanence [7, 8]. The major hysteresis loop of a system appears same, without showing clear distinction of their magnetic properties that significantly influence the final product. However, the first-order reversal curve (FORC) method, first proposed by Mayergoyz [9] and then developed by Pike [10], has become a powerful tool to study the highly interacting systems, like magnetic nanoparticles [11, 12], ferromagnetic nanowires and magnetic nanotubes [13–15]. FORC distributions are widely used to investigate the presence of magnetostatic interactions (interaction between average and individual processes taking part in aggregation of magnetic particle) and to examine the magnetization behaviour of a sample as a contribution of single-domain (SD), multi-domain (MD), pseudo-single-domain (PSD) and super-

✉ Basharat Want
basharatwant@gmail.com

¹ Solid State Research Lab, Department of Physics, University of Kashmir, Srinagar 190006, India

paramagnetic (SP) particles [16, 17]. As a matter of fact, FORC distribution not only involves interaction as entire but also provides one to separate the mean field interaction effect from local effect [18, 19]. In particular, FORC measurements have turned out to be very important in employing the purpose of the well-defined crystallographic contributions existing in the magnetic nanoparticles [20, 21]. Moreover, the FORC technique provides knowledge of the distribution of coercivities, suitable for the analysis of the reversible and irreversible contribution existing in the magnetization processes, and gives the direct evidence on the magnetostatic features of the interacting system. There is a scarcity of literature available on the magnetic behaviour of rare-earth substituted hexagonal ferrites using minor hysteresis loops, i.e. first-order reversal curves (FORCs) [22, 23]. The objective of the present work is to study the possible role of inter- and intra-particles magnetostatic interactions in Nd-substituted strontium hexaferrites using the FORC method.

2 Experimental technique

M-type Nd-substituted strontium hexaferrite nanoparticles have been prepared by citrate precursor method using analytical grade chemicals, namely ferric nitrate nonahydrate, neodymium nitrate hexahydrate, strontium nitrate anhydrous and citric acid anhydrous. Metal salts and citric acid were dissolved in a triply deionized water separately and then mixed together at room temperature with continuously constant stirring. Here, citric acid anhydrous was used as fuel. The pH of the solution was adjusted at 6.5 by using ammonia (25 %). The obtained solution was heated at 90 °C till a gel solution was obtained. The so-obtained gel was heated till combustion, ultimately leaving only loose ashes. These ashes were ground by a motor pestle arrangement for about 30 min. The whole powder was then heated at 500 °C to remove the organic moiety. Finally, the powder was calcined at 950 °C for 3 h.

The phase of the synthesized samples was determined by the D8 Advance Bruker X-ray diffractometer with $\text{CuK}\alpha$ ($\lambda = 1.5406 \text{ \AA}$) radiation. TECNAI T 20 S-TWIN transmission electron microscope was used to obtain high-resolution images to define the size and shape and corresponding selected area diffraction (SAED) pattern of the nanoparticles. The magnetic measurements, major hysteresis loops as well as first-order reversal curves, were obtained using a vibrating sample magnetometer (MicroSense EZ9 VSM) with a maximum field strength of 20 kOe.

3 Results and discussion

3.1 XRD analysis

The XRD patterns of calcined $\text{Sr}_{1-x}\text{Nd}_x\text{Fe}_{12}\text{O}_{19}$ ($x = 0, 0.05, 0.10, 0.15, 0.20$) powders are shown in Fig. 1. It is evident from the figure that almost all peaks of the hexagonal system corresponding to the space group $\text{P6}_3/\text{mmc}$ are perfectly matched with the standard pattern (JCPDS Card No. 24-1207). Some secondary phases (haematite and Nd_2O_3) are also observed from diffraction pattern, which may be present due to incomplete reaction of various reactants. It requires higher and longer sintering temperature to remove these secondary phases. The lattice parameters of all the prepared samples were compared and are given in Table 1. The lattice constant 'a' remains almost constant, while 'c' decreases with the increase in the Nd concentration. Moreover, the decrease in the parameter 'c' with substitution confirms that Nd^{3+} enters the hexaferrite lattice [24]. The decrease in lattice parameter 'c' with the increase in Nd^{3+} substitution is also reported in the literature [25]. The decrease in value of V_{cell} may be attributed to the presence of rare earth. Rare earths are known for their stability to form strong lanthanide–oxygen bonds [26]. The binding energy of lanthanide–oxygen octahedral in oxide materials is known to be much higher than that of the transition metal ion–oxygen octahedral. This may be the reason for the shrinkage of crystal lattice.

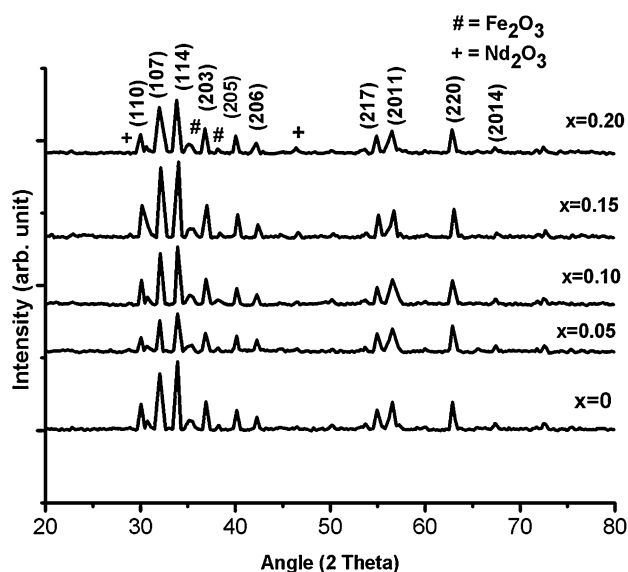


Fig. 1 Powder XRD patterns of $\text{Sr}_{1-x}\text{Nd}_x\text{Fe}_{12}\text{O}_{19}$ ($x = 0, 0.05, 0.10, 0.15, 0.20$)

Table 1 Lattice parameters and unit cell volumes of $\text{Sr}_{1-x}\text{Nd}_x\text{Fe}_{12}\text{O}_{19}$ samples

	a (Å)	c (Å)	cla	V_{cell} (Å ³)
$\text{SrFe}_{12}\text{O}_{19}$	5.92	23.23	3.92	705.51
$\text{SrNd}_{0.05}\text{Fe}_{11.95}\text{O}_{19}$	5.90	23.20	3.93	699.85
$\text{SrNd}_{0.10}\text{Fe}_{11.90}\text{O}_{19}$	5.90	23.18	3.94	699.25
$\text{SrNd}_{0.15}\text{Fe}_{11.85}\text{O}_{19}$	5.90	23.14	3.92	698.04
$\text{SrNd}_{0.20}\text{Fe}_{11.80}\text{O}_{19}$	5.89	23.15	3.93	695.98

3.2 High-resolution transmission electron microscopy

The morphology, size and the crystalline nature of $\text{Sr}_{1-x}\text{Nd}_x\text{Fe}_{12}\text{O}_{19}$ (where $x = 0.05$ and $x = 0.20$) particles were studied using a high-resolution TEM. It was observed that the average size of the nanoparticles is larger for $x = 0.05$ as compared to the composition with $x = 0.20$. The average particle size computed from the obtained images was observed to lie between 70 and 80 nm. A decreasing trend in the particle size with increasing concentration of Nd ($x = 0.05$ to $x = 0.20$) was observed in the samples of Nd^{3+} substituted strontium hexaferrite. The small size of the hexaferrite particles suggests that the system comprises of single-domain magnetic particles with sizes smaller than the critical size of 460 nm [27]. It is also clear from the TEM images that the particles aggregate to form clusters. This aggregation of particles can enhance the magnetic interaction among the particles, which may enhance the magnetic properties of $\text{Sr}_{1-x}\text{Nd}_x\text{Fe}_{12}\text{O}_{19}$ ($x = 0, 0.05, 0.10, 0.15, 0.20$) nanoparticles. Figure 2c shows the selected area diffraction pattern (SAED) and inter-planar spacing of a typical nanoparticle. The spacing between two adjacent lattice planes is 0.261 nm, which matches well with the

d value of (114) planes as obtained from the powder XRD data of the sample. So the planes visible in the TEM image belong to (114) family of planes.

3.3 Magnetic properties

Figure 3 shows the specific magnetization of $\text{Sr}_{1-x}\text{Nd}_x\text{Fe}_{12}\text{O}_{19}$ samples as a function of applied field at 25 °C. The magnetic parameters such as saturation magnetization, coercivity, remanent magnetization and anisotropy were determined experimentally and are listed in Table 2. It was observed that the saturation magnetization increases with the increase in the concentration of Nd. The obtained value of saturation magnetization is much higher than that reported for the similar materials in the literature [28]. There is no appreciable change in the values of saturation magnetization M_s with the change in Nd^{3+} concentration. The values are almost same as that of the pure strontium hexaferrite. Similar trend has also been observed by others [29, 30].

The values of squareness ratio of the prepared samples are given in Table 2. It has been reported in the literature that if the squareness ratio is equal to or greater than 0.5, the material is composed of single-domain particles and if it is below 0.5, it can be attributed to the formation of multi-domain structure [31, 32]. In the present study, the squareness ratio has been found in the range of 0.53–0.57 which shows that the prepared samples of Nd-substituted strontium hexaferrites are composed of single-domain particles. The remanent magnetization exhibits the similar trend as that of saturation magnetization. It is also observed that there is an increase in coercivity with the increase in concentration of Nd of all the prepared samples. For instance, at $x = 0.15$, the value of coercivity H_c of Nd-substituted strontium hexaferrite is 6885 Oe and that of unsubstituted sample is 6117 Oe. This means there is an

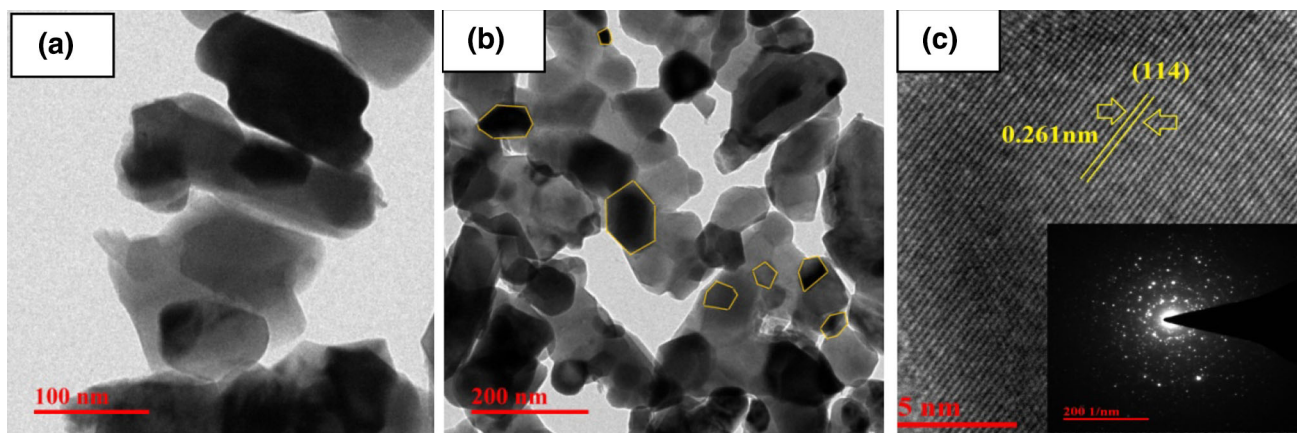


Fig. 2 TEM image for the samples **a** $\text{Sr}_{0.95}\text{Nd}_{0.05}\text{Fe}_{12}\text{O}_{19}$ **b** $\text{Sr}_{0.80}\text{Nd}_{0.20}\text{Fe}_{12}\text{O}_{19}$ and **c** Inter-planar spacing and selected area electron diffraction pattern of $\text{Sr}_{0.80}\text{Nd}_{0.20}\text{Fe}_{12}\text{O}_{19}$

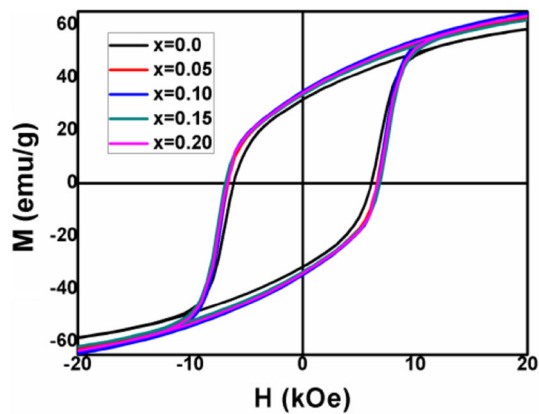


Fig. 3 Major hysteresis loop of $\text{Sr}_{1-x}\text{Nd}_x\text{Fe}_{12}\text{O}_{19}$ (where $x = 0, 0.05, 0.10, 0.15, 0.20$)

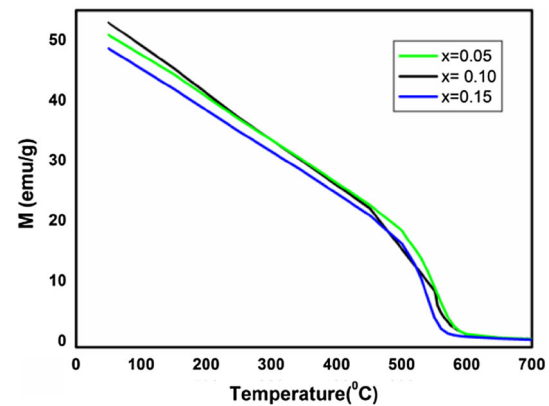


Fig. 4 Temperature-dependent magnetization of $\text{Sr}_{1-x}\text{Nd}_x\text{Fe}_{12}\text{O}_{19}$ ($x = 0.05, 0.10, 0.15$)

Table 2 Magnetic parameters of $\text{Sr}_{1-x}\text{Nd}_x\text{Fe}_{12}\text{O}_{19}$ (where $x = 0, 0.05, 0.10, 0.15, 0.20$)

	M_s (emu/g)	H_c (Oe)	M_r (emu/g)	M_r/M_s	K (HA^2/Kg)
$\text{SrFe}_{12}\text{O}_{19}$	60	6117	30.15	0.532	23.04
$\text{Sr}_{0.95}\text{Nd}_{0.05}\text{Fe}_{12}\text{O}_{19}$	63	6634	38.09	0.532	26.24
$\text{Sr}_{0.90}\text{Nd}_{0.10}\text{Fe}_{12}\text{O}_{19}$	65	6704	35.52	0.529	27.34
$\text{Sr}_{0.85}\text{Nd}_{0.15}\text{Fe}_{12}\text{O}_{19}$	63	6885	35.15	0.532	27.23
$\text{Sr}_{0.80}\text{Nd}_{0.20}\text{Fe}_{12}\text{O}_{19}$	63	6703	34.23	0.538	26.51

increase of about 12.5 % in the value of coercivity in the prepared samples. The increase in coercivity can be understood in terms of increase of anisotropy field, because coercivity is proportional to the anisotropy constant according to the following relation [33]:

$$H_c = \frac{2K}{\mu_o M_s},$$

where K is magnetocrystalline anisotropy and μ_o permeability of free space ($= 4\pi \times 10^{-7}$ H/m). The increase in coercivity and the increase in substitution of Nd concentration (up to $x = 0.15$) may be related to the increase in the magnetocrystalline anisotropy K (see Table 2) and decrease in the grain size as shown in TEM images (Fig. 2). The magnetoanisotropy constant K obtained for the $\text{Sr}_{0.90}\text{Nd}_{0.10}\text{Fe}_{12}\text{O}_{19}$ is much more than that of bulk single crystal [34] which is in good agreement with the already proposed theory by Bodker et al. [35]. According to this theory, hexagonal particles are observed to exhibit higher magnetoanisotropy constant than bulk single crystals. It is reported that recording media requires high enough coercivity of around 600 Oe, but for perpendicular magnetic recording media it requires coercivity above 1200 Oe [36]. In the present study, the obtained coercivity of the synthesized samples lies in the range of 6601 Oe to 6884 Oe which may be useful for magnetic recording media and is highest than already reported in the literature [37–39]. The

results obtained on coercivity of Nd-substituted strontium hexaferrite in the present study are close to the theoretical limit of (7.5 kOe) [40].

3.4 Curie temperature measurements

Measurement of Curie temperature, T_c , of the prepared Nd-substituted strontium hexaferrite samples was carried out using a high temperature facility attached with the vibrating sample magnetometer (MicroSense EV9 VSM). Figure 4 shows the variation of magnetization as a function of temperature for all the prepared samples. It shows a normal behaviour of decrease in magnetization with the increase in temperature with dip at Curie point.

The Curie temperature, calculated from the curves, decreases as Nd^{3+} concentration increases. The behaviour is a normal one and is reported by various researchers [41, 42]. The decrease in T_c indicates that some exchange interactions (RE–O–TM and TM–O–TM) get weaker and weaker as the Nd^{3+} concentrations increase. The reason for this weakening of exchange interactions can be attributed to the conversion of strong magnetic ions (Fe^{3+}) into weak ones (Fe^{2+}) upon Nd^{3+} substitution [43]. Therefore, it is expected that a greater amount of energy will be required to offset the effects of exchange interactions in the materials having stronger magnetic ions.

3.5 First-order reversal curve (FORC) analyses

FORC measurement starts with saturating a sample by applying a large magnetic field H_b . Then, the field is lowered down to a reversal field H_a . A partial hysteresis curve (a FORC) is measured as the applied magnetic field H_b increases from H_a back to saturation. This process of measurement is repeated for a number of values H_a to get a set of FORCs. The magnetization at any applied magnetic field H_a along the reversal curve with reversal field H_a is represented by $M(H_a, H_b)$, where $H_b > H_a$. The FORC method provides the information regarding the switching field distribution and gives an insight of the interaction mechanism among the particles in the system [13]. FORC contours are developed by calculating second-order derivative of the following equation.

$$\rho(H_a, H_b) = -\frac{\partial^2 M(H_a, H_b)}{\partial H_a \partial H_b}$$

The local coercivity field (H_c) and bias interaction field (H_u) are generated by a coordinate transformation: $H_c = (H_b - H_a)/2$ and $H_u = (H_b + H_a)/2$. FORC diagrams resemble normally with the known Preisach diagrams [8]. Any hysteretic process can be identified using a FORC diagram. It has been reported that FORC can be modelled as collection of components [44–46], indicating that the individual contribution of multiple phases can be recognized. Identification between single-domain and multi-domain behaviour is straightforward using FORC diagram.

Figure 5a represents first-order reversal curves obtained at room temperature. The FORC data were converted into FORC diagram using the FORCinel software [47]. A small amount of smoothing is always required in the calculation of FORC distribution from experimental data: the level of smoothing is defined by a smoothing factor (SF). A smoothing factor of three, which was the optimal smoothing factor for the majority of samples, was used for all diagrams. In the FORC diagrams, horizontal axis represents coercive field H_c , which is sensitive to the particle size and composition, whereas vertical axis H_u gives us the information on magnetic interaction among particles [18]. The FORC distribution contours enable us to study different features of the prepared samples and also to find some surprising aspects in the reversal curves, which are hard to recognize with the major hysteresis loop. From the FORC diagrams, a single peak is observed in each sample which is almost similar and is related to the irreversible contribution of the magnetization. It may be noted that these peaks are from hard magnetic phases with a coercivity of around 7500–7800 Oe [48]. The coercivity obtained by FORC analysis is larger than the coercivity obtained from the major hysteresis loop of Nd^{3+}

substituted strontium hexaferrite samples. The observed distribution of coercivity in the FORC diagrams proves itself the evidence for the existence of a size distribution of the nanoparticles. For the substitution at $x = 0.20$, a small secondary peak is observed near about the origin of the FORC diagrams which can be assigned to the haematite phase. Therefore, due to the formation of these small secondary peaks, a decrease in the total coercivity results. The decrease in coercivity due to the presence of haematite phase is also in accordance with the major hysteresis loop results. Careful analysis of the FORC distribution of all three samples indicates close concentric contours around the central peaks, which is a typical behaviour of single-domain nanoparticles.

For the substitution at $x = 0.10, 0.15, 0.20$, the FORC distribution shows clear pattern in the form of a peak stretching along H_c and H_u . Such kind of characteristic is typical of aggregation (cluster) of single-domain nanoparticles where the distributed peaks in ρ along H_c correspond to the distribution of coercivities in the prepared samples (because of particle size distribution) and the distributed peaks along H_u show the distribution of bias fields, i.e. the amount of inter-particle interaction. This is a typical feature of a system which is composed of an aggregation of single-domain particles with moderate interaction and a wide size distribution [11]. Moreover, in the FORC diagrams, an additional feature, i.e. negative region, is also observed which signifies that the materials under consideration are of single domains [49, 50].

In order to assess and summarize various FORC diagrams (as shown in the Fig. 5b) obtained for different samples, a statistical analysis was carried out for the profiles of both interaction and coercive field distributions for all samples. For the sake of consistency, the coercive field and interaction fields were best fit by Gaussian distribution. The results suggest that the samples contain large part of hard magnetization which produces wide Gaussian distribution and small particles clusters are formed. Within these clusters, there is strong interaction among the particles. From the FORC diagram, it can be observed that the coercivity distributions for the samples $x = 0.10$ and 0.15 are larger than the sample $x = 0.20$. A significant increase in the coercivity of the sample substituted at $x = 0.10$ and 0.15 is due to the presence of only hard phase, while for $x = 0.20$, the sample contains soft phase in addition to hard phase. The average H_c is 7317 Oe, 7559 Oe and 7426 Oe. More importantly, the width of H_c distribution is 787.5 ± 5.6 , 820.5 ± 2.37 and 748.6 ± 6.96 , respectively. The broader distributions of coercive field are expected from the hard coupling. The observed enhancement in both coercive field and interaction field with increasing Nd content has an impact on the higher frequency behaviour of the material. The large vertical spread in H_u (Fig. 5b)

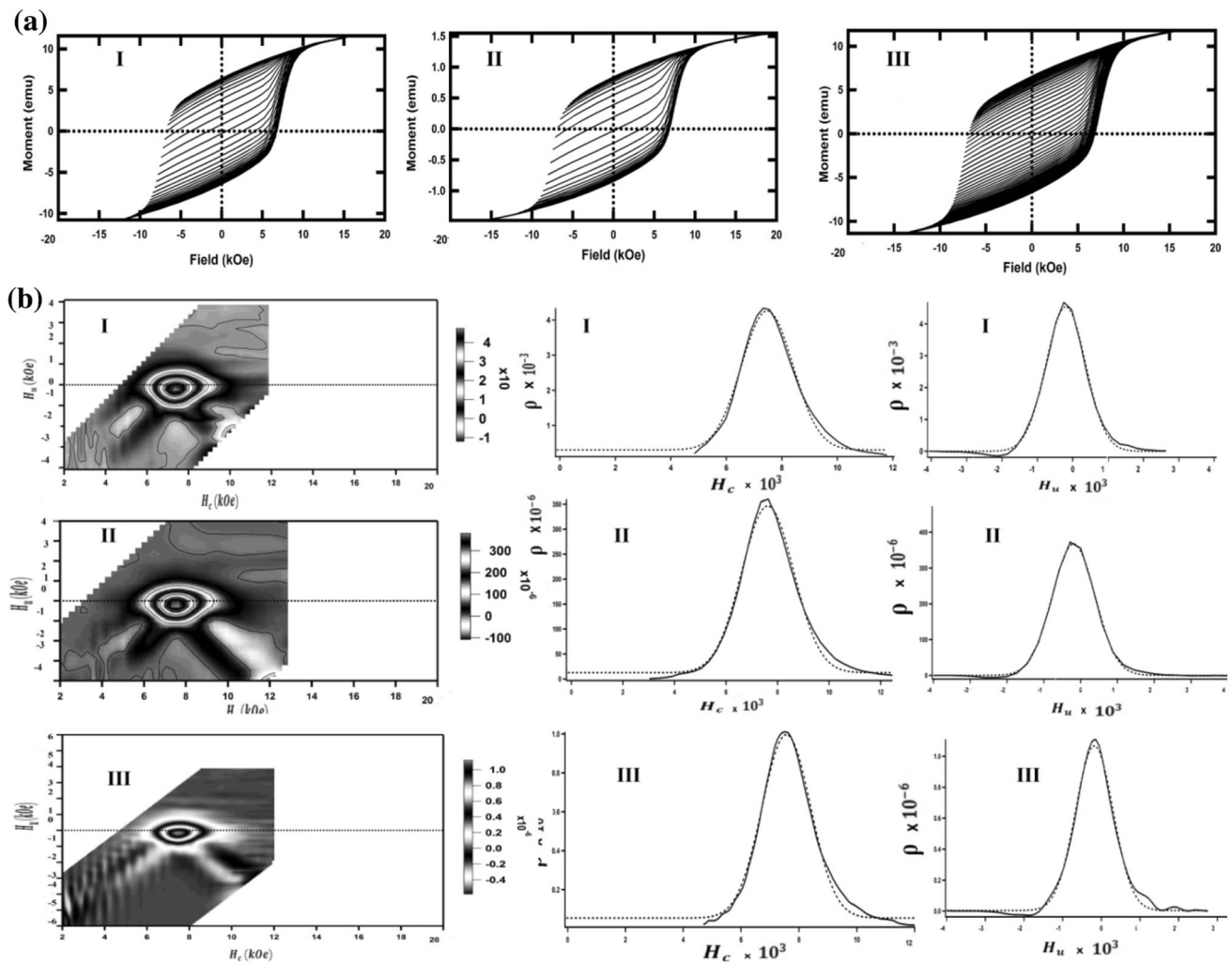


Fig. 5 **a** First-order reversal curves for $\text{Sr}_{1-x}\text{Nd}_x\text{Fe}_{12}\text{O}_{19}$ (I) $x = 0.10$ (II) $x = 0.15$ (III) $x = 0.20$. **b** FORC diagrams and the corresponding FORC density distribution profiles showing the coercivity distribution

and interaction field for the prepared samples: $\text{Sr}_{1-x}\text{Nd}_x\text{Fe}_{12}\text{O}_{19}$ (where $x = 0.10, 0.15, 0.20$)

suggests that there is strong magnetic interaction among the particles, and thus, aggregation of particles is formed. This result is consistent with the TEM observations. This aggregation behaves like as single-domain particles, leading to higher coercive force. However, for the sample doped at $x = 0.20$ [as shown in the Fig. 5b (III)], the projection of FORC distribution on to H_u , it is observed that there is a decrease in peak width when centred at 0 Oe. This suggests that the interaction among the particles becomes weaker.

4 Conclusions

In this work, the influence of Nd doping on the structural and magnetic properties of $\text{Sr}_{1-x}\text{Nd}_x\text{Fe}_{12}\text{O}_{19}$ ($x = 0, 0.05, 0.10, 0.15, 0.20$) has been investigated systematically.

XRD analysis of all the samples showed the hexagonal phase characteristic of the $\text{SrFe}_{12}\text{O}_{19}$ crystal structure. It was observed that there is a slight decrease in the lattice constant 'c', whereas lattice constant 'a' almost remains constant. TEM analysis showed that the particles are in the nanorange. It was found that there is no significant variation in saturation magnetization, while the coercivity increases with the increase in Nd^{3+} concentration. The Curie temperature decreased with the increase in Nd concentration. In FORC analysis, a peak was observed in each sample that can be associated with the irreversible part of the magnetization. First curve analysis showed that the coercivity was much more than the conventional major hysteresis loop. From the FORC diagram, the broader distributions of coercive field are expected from the hard coupling, while the FORC interaction distribution indicates the strong magnetic interaction between the particles and,

thus, the formation of small clusters that act as single domain. The presence of haematite in the sample doped at $x = 0.20$ narrows the FORC interaction field distribution when compared to the sample at $x = 0.10, 0.15$. These results demonstrate that the FORC technique is a powerful tool to analyse the magnetic properties of magnetic materials such as hexaferrite.

Acknowledgments The author Basharat Want is highly thankful to the authorities of University of Kashmir for providing a vibrating sample magnetometer facility (VSM Model EZ9, make USA) under DST, Govt. of India, special package for sophisticated instruments. The author is also grateful to Prof. Manzoor Malik, HOD Physics, for facilitating the procurement of the VSM facility.

References

- R.C. Pullar, Prog. Mater. Sci. **57**, 1191 (2012)
- A. Haq, M. Anis-ur-Rehman, Phys. B **407**, 822–826 (2012)
- M. Kaiser, Curr. Appl. Phys. **10**, 975–984 (2010)
- L. Lechevallier, J.M. Le Breton, J.F. Wang, I.R. Harris, J. Magn. Magn. Mater. **269**, 192–196 (2004)
- S. E. Rowley, Y. S. Chai, S. P. Shen, Y. Sun, A. T. Jones, B. E. Watts, J. F. Scott, arXiv condmat: 1507.01880v2 (2015)
- J. F. Scott, npj Compumats. doi:10.1038/npjcompumats.2015.6
- Y.C. Sui, R. Skomski, K.D. Sorge, D. Sellmyer, Appl. Phys. Lett. **84**(9), 1525–1527 (2004)
- M. Zheng, R. Skomski, Y. Liu, D. Sellmyer, J. Phys. Condens. Matter **12**, L497 (2000)
- I.D. Mayergoyz, IEEE Trans. Magn. **22**, 603–608 (1986)
- C.R. Pike, A.P. Roberts, K.L. Verosub, J. Appl. Phys. **85**, 6660–6662 (1999)
- R. Lavín, J.C. Denardin, J. Escrig, D. Altbir, A. Cortes, H. Gomez, IEEE Trans. Magn. **44**(1), 2808 (2008)
- F. Brem, L. Tiefenauer, A. Fink, J. Dobson, A. Hirt, Phys. Rev. B **73**, 224427 (2006)
- I. Ursachi, A. Vasile, H. Chiriac, P. Postolache, A. Stancu, Mater. Res. Bull. **46**, 2468–2473 (2011)
- M.P. Proenca, C.T. Sousa, J. Escrig, J. Ventura, M. Vazquez, J.P. Araujo, J. Appl. Phys. **113**, 093907-7 (2013)
- F. Beron, D. Menard, A. Yelon, J. Appl. Phys. **103**, 07D908-3 (2008)
- R. Lavín, J.C. Denardin, J. Escrig, D. Altbir, A. Cortés, H. Gómez, IEEE Trans. Magn. **44**, 2808 (2008)
- C. Carvallo, A.R. Muxworthy, D.J. Dunlop, W. Williams, Earth Planet Sci. Lett. **213**, 375–390 (2003)
- M.P. Proenca, C.T. Sousa, J. Escrig, J. Ventura, M. Vazquez, J.P. Araujo, J. Appl. Phys. **113**, 093907-7 (2013)
- H. Chiriac, N. Lupu, L. Stoleriu, P. Postolache, A. Stancu, J. Magn. Magn. Mater. **316**, 177–180 (2007)
- L.G. Vivas, M. Vazquez, J. Escrig, S. Allende, D. Altbir, D.C. Leitao, J.P. Araujo, Phys. Rev. B **85**, 035439 (2012)
- M. Ciureanu, M.F. Beron, P. Ciureanu, R.W. Cochrane, D. Menard, A. Sklyuyev, A. Yelon, J. Nanosci. Nanotechnol. **8**, 5725–5732 (2008)
- M. Zheng, R. Skomski, Y. Liu, D. Sellmyer, J. Phys. Condens. Matter **12**, 497 (2000)
- P.G. Bercoff, H.R. Bertorello, J. Magn. Magn. Mater. **320**, e100–e103 (2008)
- Q.Q. Fang, H. Cheng, K. Huang, J. Wang, R. Li, Y. Jiao, J. Magn. Magn. Mater. **294**, 281–286 (2005)
- J. Luo, Mater. Lett. **80**, 162–164 (2012)
- S. Cotton, Lanthanide actinide chemistry, vol. 5 (John Wiley Sons Ltd., UK, 2006), p. 61
- L. Rezlescu, E. Reslescu, P.D. Popa, N. Rezlescu, J. Magn. Magn. Mater. **193**, 288–290 (1999)
- Z. Zhang, X. Liu, X. Wang, Y. Wu, R. Li, J. Magn. Magn. Mater. **525**, 114–119 (2012)
- X. Liu, W. Zhong, S. Yang, Z. Yu, B. Gu, Y. Du, J. Magn. Magn. Mater. **238**, 207 (2002)
- X. Liu, W. Zhong, S. Yang, Z. Yu, B. Gu, Y. Du, Phys. Stat. Sol. (a) **193**(2), 314 (2002)
- C. Sudakar, G.N. Subbanna, T.R.N. Kutty, J. Magn. Magn. Mater. **263**, 253–268 (2003)
- M.N. Ashiq, M.F. Ehsan, M.J. Iqbal, M. Najam-ul-Haq, J. Magn. Magn. Mater. **332**, 93 (2013)
- E.C. Stoner, E.P. Wohlfarth, I.E.E.E. Trans. Mag. **273**, 475–3518 (1991)
- B. Shirk, W.R. Buessem, J. Appl. Phys. **40**, 1294–1296 (1969)
- F. Bodker, S. Morup, S. Linderth, Phys. Rev. Lett. **72**, 282–285 (1994)
- Y. Li, R. Liu, Z. Zhang, C. Xiong, Mater. Chem. Phys. **64**, 256–259 (2000)
- A. Thakur, R.R. Singh, P.B. Burman, Mater. Chem. Phys. **141**, 562–569 (2013)
- T. Kaul, S. Kumar, B.H. Bhat, B. Want, A.K. Srivastava, Appl. Phys. A **119**(4), 1531–1540 (2015)
- B. Want, B.H. Bhat, Z.A. Bhat, J. Alloys. Compd. **627**, 78–84 (2015)
- V.V. Pankov, M. Pernet, P. Germi, P. Mollard, J. Magn. Magn. Mater. **120**, 69 (1993)
- B.K. Rai, S.R. Mishra, V.V. Nguyen, J.P. Liu, J. Magn. Magn. Mater. **581**, 275–281 (2013)
- M. Sivakumar, A. Gedanken, W. Zhong, Y.W. Du, D. Bhattacharya, Y. Yeshurun, J. Magn. Magn. Mater. **268**, 95–104 (2004)
- X. Liu, W. Zhong, S. Yang, Z. Yu, B. Gu, Y. Du, J. Magn. Magn. Mater. **238**, 207–214 (2002)
- C.R. Pike, C.A. Ross, R.T. Scalettar, G. Zimanyi, Phys. Rev. B **71**, 134407 (2005)
- A. Stancu, P.K. Pike, L. Stolriu, P. Postolache, D. Cimpoesu, J. Appl. Phys. **93**, 6620 (2003)
- C.R. Pike, A.P. Robert, D.J. Dunlop, W. William, Earth Planet Sci. Lett. **213**, 375 (2003)
- R. J. Harrison, Geochem. Geophys. Geosyst., Q05016, doi: 10.1029/2008GC001987
- J. Nicolas, in Microwave ferrites, in ferromagnetic materials, vol. 2, ed. by E.P. Wohlfarth (North-Holland, Amsterdam, 1987), pp. 243–296
- A.R. Muxworthy, D. Heslop, W. Williams, Geophys. J. Int. **158**, 888–897 (2004)
- C.R. Pike, Phys. Rev. B **68**, 104424–104425 (2003)